Edinburgh Research Explorer

Robust natural nanocomposites realizing unprecedented ultrafast precise molecular separations

Graphical abstract

Robust natural nanocomposites realizing unprecedented ultrafast precise molecular separations

pp xxx–xxx

Yanqiu Zhang, Xiquan Cheng, Xu Jiang, Jeffrey J. Urban, Cher Hon Lau [*], Shaoqin Liu, Lu Shao [*]
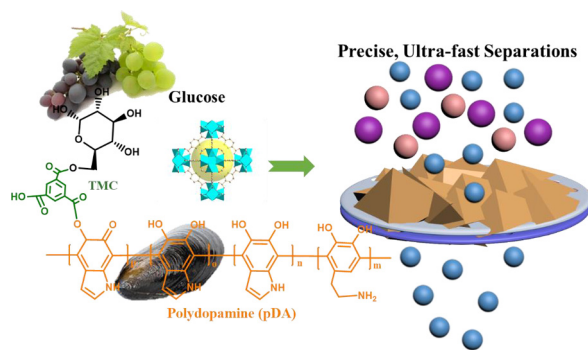
A facile technique to combine natural compounds and metal organic frameworks (MOFs) that produces a well-structured membrane with unparalleled separation performances was designed. Our synthesized membrane enables ultra-fast, low-pressure, precise separations for both solvent purification via organic solvent nanofiltration and desalination – key membrane-based processes for efficiently tackling worldwide water crisis.

Highlights

• Natural-driven nanocomposite membranes was first fabricated. • A sub-214 nm-thick selective layer was synthesized by natural materials. • The novel membrane has an extraordinary stability even in strong solvent environment. • The membranes exhibited high rejection against angstrom-sized contaminants.

RESEARCH: Original Research

Robust natural nanocomposites realizing unprecedented ultrafast precise molecular separations

Yanqiu Zhang[1], Xiquan Cheng[2], Xu Jiang[1], Jeffrey J. Urban[3], Cher Hon Lau[4],*, Shaoqin Liu[5], Lu Shao[1],*

[1] MIIT Key Laboratory of Critical Materials Technology for New Energy Conversion and Storage, State Key Laboratory of Urban Water Resource and Environment (SKLUWRE), School of Chemistry and Chemical Engineering, Harbin Institute of Technology Harbin 150001, China
[2] School of Marine Science and Technology, Sino-Europe Membrane Technology Research Institute, Harbin Institute of Technology Weihai 264209, China
[3] The Molecular Foundry, Lawrence Berkeley National Laboratory, Berkeley, CA 94720, United States
[4] School of Engineering, The University of Edinburgh, The King's Buildings, Mayfield Road, EH9 3JL, United Kingdom
[5] School of Life Science and Technology State Key Laboratory of Urban Water Resource and Environment Harbin Institute of Technology, Micro- and Nanotechnology Research Center Harbin Institute of Technology Harbin 150080, China

Synthetic polymer membranes can potentially reduce the large energy and carbon footprints that are typically associated with traditional chemical separation technologies. Unfortunately, current production protocols negate the green benefits of membrane separation. To address this bottleneck, here we report the use of natural materials monosaccharide – glucose and polydopamine and Zr-based metal organic frameworks (MOFs) to fabricate ultrathin nanocomposite membranes *via* interfacial polymerization reaction. The synergistic effect of these three materials on angstrom-scale molecular transport both in organic solvent and aqueous environment was elucidated using a series of complementary techniques. We demonstrate such nature-inspired nanocomposite membranes enable structural stability even in polar aprotic solvents, and unparalleled ultra-fast, low-pressure, precise separations in both nanofiltration modes, which easily surpass state-of-the-art membranes relying on unsustainable materials. The multi-functionality of saccharide nanocomposites was elegantly harnessed to impact separation applications that contribute towards a better living environment.

Keywords: Nanoporous membrane; Sustainable natural materials; Nanofiltration; Desalination; Metal organic frameworks

Introduction

Advanced separation techniques are crucial for environmental remediation where industrial wastewater is treated before discharge and in the production of potable water to address water scarcity that affects two-thirds of the global population around 4 billion people [1]. The principle underpinning separation processes in these applications is based on the removal of molecular compounds such as heavy metal ions, dyes, and salts from water and organic liquids using a driving force. This can be achieved with a phase change where the liquid is boiled off leaving the molecular solids behind i.e. distillation [2]. Alternatively, pressure can be employed as a driving force to achieve the same effect using membranes, but with significantly lower energy consumption (as much as 90% lower) [3,4]. To realize this potential, membranes must have excellent transport characteristics, and maintain separation regardless of operating conditions and environment [5].

* Corresponding authors.
    E-mail addresses: Lau, C.H. (cherhon.Lau@ed.ac.uk), Shao, L. (shaolu@hit.edu.cn).

1

The first commercial polymer membrane was fabricated in the 1960s using cellulose acetate, a functionalized natural polymer, for the production of potable water *via* reverse osmosis desalination [6]. With excellent chemical resistance, cellulose acetate membranes were initially preferred for commercial settings. However, the production of cellulose acetate was extremely difficult when compared to synthetic polymers. Hence, there was a shift towards using synthetic polymers derived from fossil fuel resources for membrane separations. As fossil fuel becomes depleted, there is a need to revisit the use of natural, renewable materials for optimizing the green benefits of advanced separation technique [7]. This strategy draws inspiration from the ongoing replacement of polystyrene or polyethylene packaging with biodegradable poly(lactic acid) [8], and is best demonstrated with cellulose membranes for purifying water/oil mixtures [9]. However, this approach is seldom demonstrated for organic solvent nanofiltration (OSN) [10,11] as most natural materials are unstable in polar organic solvents and whilst demonstrating low solvent permeances. For example, polyesters derived from gallic acid and polyamides produced from tannic acid demonstrated good water permeances and excellent selectivity towards inorganic salts but were not resistant to organic solvents [12]. Likewise, membranes fabricated from polydopamine (pDA), a mussel-inspired polyphenol material with strong adhesion onto almost all kinds of substrates, have attracted extensive interest primarily due to good salt resistances whilst remaining stable in organic liquids, enabling applications in organic solvent nanofiltration [13,14]. However, pDA-derived membranes typically have low solvent flux as crosslinking was required to ensure the chemical stability of pDA in organic solvents. Clearly, there remains a trade-off relationship between chemical stability and separation performances of membrane derived from natural compounds.

Enhancing separation performance of traditional polymeric membranes can be achieved with the combination of various compatible nano-fillers [15–19], such as metal organic frameworks (MOFs). MOFs are crystalline materials comprising metal ions linked together by organic ligands [20,21] which are deployed in this study for their exceptional porosity that can enhance solvent transport by propping polymer chains further apart, or through their intrinsic porosity [17,18]. The selectivity of MOF-based nanocomposite membranes towards targeted molecules can be enhanced by tailoring MOF affinity for these molecules or by optimizing inter-polymer chain distance to maximize the transport of a target molecule [22]. MOFs like HKUST (Cu-based MOFs) and ZIF-8 (Zn-based MOFs) can enhance membrane permeability during liquid separations. However, the poor hydrostability of HKUST impedes the application of resultant membranes for water separations [23,24] while the small intrinsic pores of ZIF-8 (about 0.32 nm) restricts the transport of larger organic solvent molecules such as alcohols, ketones, and acetates [25]. Interestingly, Zirconium (IV)-carboxylate MOFs (Zr-MOFs) such as UiO-66 type MOFs do not suffer from these limitations of typical MOF fillers and exhibit exceptional chemical and thermal stabilities even in NaOH and HCl solutions. This is ascribed to strong coordination bonds between the hard-acid-hard-base
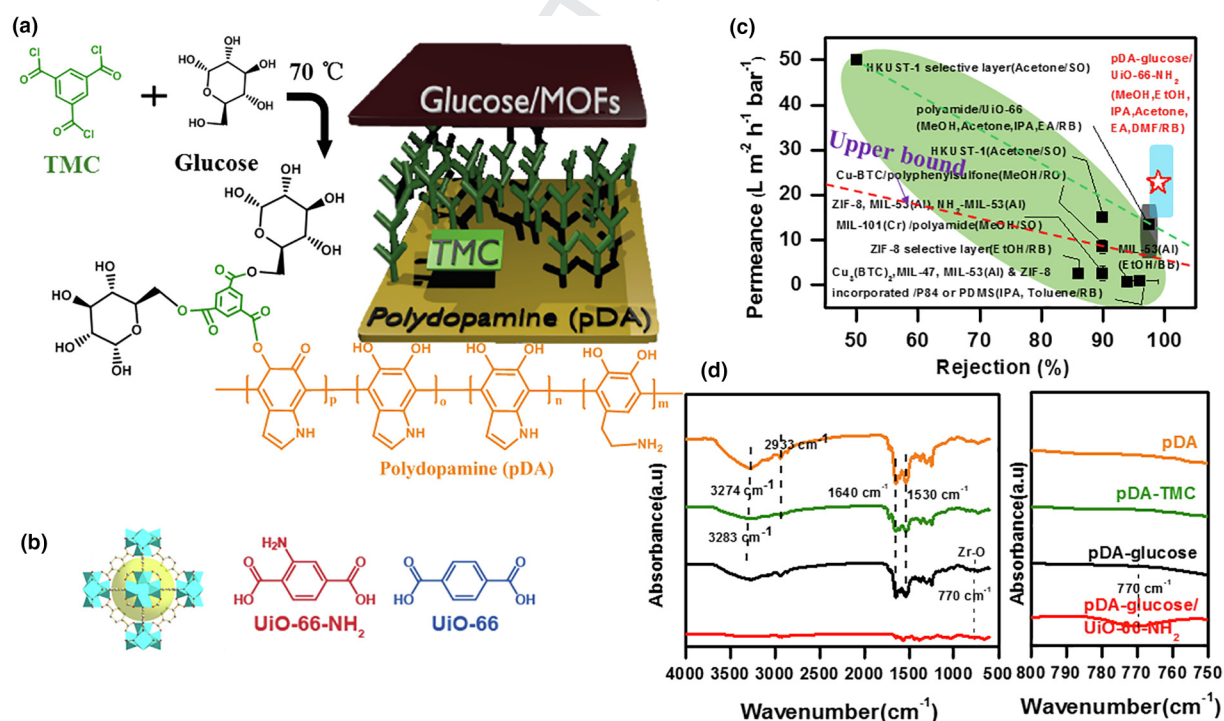
FIGURE 1

(a) Cartoon showing the different components in the selective layer (pDA, glucose and MOFs) and porous substrate or support (polyimide) of the ultrathin composite membranes studied in this work. The thickness of the selective layer is about 214 nm. (b) Chemical structures of UiO-66 and UiO-66-NH$_2$. (c) A comparison of separation performances of pDA–glucose/MOF membranes developed in this work and state-of-the-art MOF-based nanocomposite membranes for organic solvent nanofiltration. (d) FTIR analyses of pDA, pDA–TMC, pDA–glucose and pDA–glucose/MOFs ultrathin nanocomposite membranes (8 h pDA coating).

interactions between the Zr (IV) atom and carboxylate oxygen [26]. Theoretically, Zr-MOFs like UiO-66-NH$_2$ and UiO-66 are ideal fillers for improving molecular separations with polymer membranes [26,27]. In reality, this remains an unaccomplished target as the interface between soft materials such as polymers and hard crystalline fillers i.e. MOFs are extremely difficult to compatibilist; leading to membranes with high permeance and low selectivity.

Different from these approaches, here, we report that the combination of natural materials – glucose and pDA with Zr-based MOFs *via* interfacial polymerization reaction can produce high-performance, multi-functional nanofiltration membranes for organic solvent nanofiltration where molecular dyes (Fig. S1 and Table S1) are separated from organic liquids during solvent recovery and in desalination to remove inorganic salts from water (Fig. 1a,b). We show here that each component of this nanofiltration membrane is crucial for yielding excellent separation performances in different media without sacrificing both selectivity and chemical stability at various operating conditions. The separation performances of our novel nanocomposite membrane derived from natural compounds outperformed state-of-the-art MOF-based nanocomposite membranes (Fig. 1c and Table S2) [17,23,24,28–30] and were two orders of magnitude higher than that of commercially OSN membranes [31]. This was mainly ascribed to the synergistic effects of each component that overcome the traditional drawbacks of each material – poor chemical stability, low solvent permeance and reduced selectivity. Importantly, our strategy can be extended to other natural compounds with compatible functionality to produce next-generation membranes with a plethora of combinations.

Experimental methods

Thin-film nanocomposite (TFN) selective layer

Porous polyimide (PI) substrates were prepared *via* a phase-inversion process as shown in Fig. S2 [32]. PI substrates were incubated in 100 mL Tris(hydroxymethyl)amino methane (Tris-HCl) buffer solution contained 0.2 g of dopamine hydrochloride for certain time. These pDA-loaded PI substrates were washed thoroughly with water. Consequently, the membrane was dried in air and covered with 0.2% (w/v) 1,3,5-benzenetricarbonyl trichloride (TMC) hexane solution for 3 minutes. This pDA–TMC membrane was rinsed twice with n-hexane to remove excessive TMC. We then poured a 2% (w/v) glucose aqueous solution containing 0.2% (w/v) UiO-66-NH$_2$ or UiO-66 and 0.27% (w/v) 4-dimethyl-aminopyridine (DMAP) onto the surface of pDA–TMC membrane. The glucose/MOF mixtures were stirred for more than 24 h to ensure uniform solutions with finely dispersed Zr-MOFs prior deposition on the pDA-loaded PI substrate. The glucose/MOF mixture was allowed to rest on the pDA–TMC surface for 5 min. This facilitated the interpenetration of glucose/MOF solutions within the pDA layer. After 5 min, the glucose/MOF nanocomposite on the topmost surface of the pDA–TMC membrane was cured at 70 °C for 15 min – allowing nucleophilic reactions between TMC acyl chlorides and glucose hydroxyl groups. Unreacted glucose was washed from the pDA–glucose/MOF selective layer with deionized water. A similar approach was adopted for a control sample without MOFs.

Results and discussion

As a proof-of-concept, we employed pDA–glucose/MOF nanocomposites as 200–300 nm ultrathin selective layers of composite membranes comprising porous polyimide supports (Fig. 1a and b). Glucose was chosen here for its availability, low-cost, hydrophilicity and low molecular weight that can possibly reduce the formation of non-selective voids during interfacial polymerization. MOFs were porous crystalline materials comprising metal ions linked together by organic ligands [20,33], and were deployed here for their exceptional porosity that drastically enhanced solvent transport [17]. UiO-66 and UiO-66-NH$_2$ MOFs [34,35] were chosen here for their stability in water and organic solvents. These Zr-based MOFs can also be produced at room temperature using acceptable solvents;[36] potentially contributing towards the fabrication of a green membrane. The remarkable adhesion properties of pDA [37] was harnessed here to prevent delamination of the glucose/MOF selective layer from the porous substrate and restrain macroscopic cracks during membrane fabrication. These materials were assembled into a thin selective layer *via* interfacial polymerization. This approach was adopted to produce ultrathin nanofiltration membranes with excellent molecular transportation properties. Fourier transform infra-red spectroscopy (FTIR) was deployed to verify the presence of these MOF in 214 ± 10 nm ultrathin pDA–glucose/UiO-66-NH$_2$ selective layers. Upon pDA deposition, new peaks centered at 3274 cm^{-1} and 2933 cm^{-1} were observed from the FTIR analyses (Fig. 1d). The peak at 3274 cm^{-1} correlated to the stretching vibrations of both pDA amine and phenolic –OH groups, while the peak at 2933 cm^{-1} corresponded to the –CH$_2$– stretch in pDA. Aromatic rings of pDA contributed to peaks at 1640 cm^{-1} and 1530 cm^{-1} [38]. To facilitate subsequent coupling of glucose and MOFs, we grafted trimesoyl chloride on to the pDA layer. This was evidenced by a blue-shift of the peak at 3274 cm^{-1} to 3283 cm^{-1}, whilst the intensity of this peak was reduced drastically. This peak was broadened further when glucose was coupled on to the pDA–TMC membrane surface. This was due to the introduction of more –OH groups by the reaction between glucose hydroxyl group with TMC acyl chlorides or pDA. In the presence of UiO-66-NH$_2$ MOFs, new peaks at 770 cm^{-1} corresponding to Zr-O bonds were also observed [39]. X-ray photoelectron spectroscopy validated the presence of these elements (Fig. S3 and Table S3) in pDA–glucose/UiO-66-NH$_2$ selective layers (Fig. 2a). MOFs used here in this work were synthesized according to the work of Farha and co-workers (Fig. S4) [34]. X-ray diffraction (XRD) analyses of these MOFs consisted peaks centered at 2θ positions that were characteristic of UiO-family MOFs (Fig. S5). The textural properties and particle size of our Zr-MOFs were also shown in Table S4, Fig. S6 and Fig. S7.

In the presence of glucose, the homogeneous distribution of Zr element was clearly observed by SEM (Fig. 2b), EDS spectrum (Fig. S8) and element mapping of pDA–glucose/UiO-66-NH$_2$ composite membranes, which illustrated that UiO-66-NH$_2$ MOFs nanoparticles were finely dispersed in the selective layer not the UiO-66 (Fig. 2b and c). This was due to the formation of hydrogen bonds and the amide bonds between the hydroxyl functional groups of glucose and amine groups of UiO-66-NH$_2$
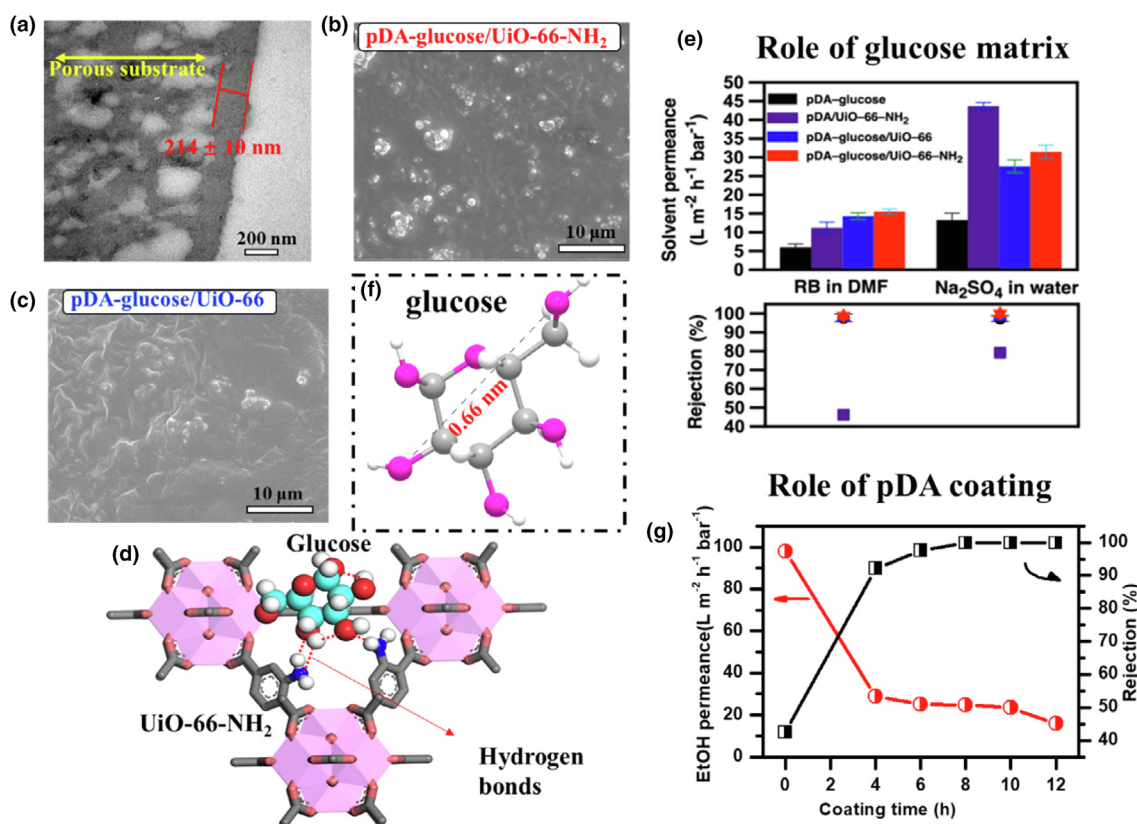
3

FIGURE 2

(a) The average thickness of the pDA–glucose/MOF selective layers is around 214 nm (8 h pDA coating). (b and c) The dispersion of UiO-family MOFs is dependent on the functional groups present. Hydrophilic NH$_2$ functional groups facilitate the dispersion of these Zr-based MOFs, while pristine UiO-66 MOFs tend to agglomerate. (d) MD simulations of glucose and UiO-66-NH$_2$ MOFs showed the preferred interactions between these components *via* hydrogen bonding. Hydrogen bonds formed between glucose and UiO-66-NH$_2$ segments. (Zr., pink; O in UiO-66-NH$_2$, magenta; C in UiO-66-NH$_2$, black; N, blue; C in glucose, cyan; O in glucose, red; H in glucose, white; H atoms connected to C in UiO-66-NH$_2$ were not shown.) (e) The roles of glucose matrix are elucidated with organic solvent nanofiltration experiments using DMF and Rose Bengal (RB) dyes at room temperature and 5 bar and nanofiltration tests with Na$_2$SO$_4$ and water with 8 h pDA coating. (f) Glucose molecular size is calculated using Chem 3D. (g) The roles of the pDA coating time are elucidated with organic solvent nanofiltration experiments using ethanol and RB at room temperature.

MOFs. This was evidenced by FTIR analyses (Fig. S9) where the three —NH—C=O new peaks at 2940 cm^{-1} and 1646 cm^{-1} appeared and the relative intensities of peaks centered at 3451 cm^{-1} (—OH of glucose) were enhanced and red-shift after UiO-66-NH$_2$ nanoparticles interaction with glucose. Molecular dynamics simulations (Fig. 2d) validated preferential interactions between glucose and the —NH$_2$ functional groups where three hydrogen bonds were observed [40]. Without —NH$_2$ functional groups, UiO-66 agglomerated within the pDA–glucose matrix. Clearly, the amine functional groups were crucial for the better interactions between the MOF additives and pDA–glucose matrix. This was elucidated here with gas adsorption analysis of UiO-66 and UiO-66-NH$_2$ MOFs blended with glucose. When blended with glucose, the surface area of UiO-66 MOFs was reduced only by 10% from 1410 m^2 g^{-1} to 1257 m^2 g^{-1} (Table S5). This loss in surface area was significantly smaller than the 32% loss in surface area of glucose/UiO-66-NH$_2$ blends and could be due to the interpenetration of glucose chains within the MOF pores.

To further demonstrate the role of glucose, we fabricated a pDA/MOF membrane, and compared its separation performances with similar membranes that contained glucose (Fig. 2e and Fig. S10). However, this was only feasible with UiO-66-NH$_2$ MOFs where only small amounts of UiO-66-NH$_2$ MOFs were deposited on to the pDA layer. This was due to the membrane fabrication protocol adopted here. At room temperature, there was insufficient energy to immobilize these MOFs at the membrane surface, whereas high temperatures [41] were mandatory for incorporating MOFs on to membrane surfaces or *via* simple physical blending with readily produced polymers [42–44]. Moreover, in our approach, UiO-66-NH$_2$ were unable to directly react with pDA due to the TMC intermediate layer. With a low concentration of UiO-66-NH$_2$, the RB/DMF and Na$_2$SO$_4$/water separation performances (rejection) of pDA/UiO-66-NH$_2$ MOF membranes were lower than membranes that also contained glucose (Fig. 2e). The improved hydrophilicity and tunable surface charges of the separation layers by grafting a glucose molecule will lead to a high nanofiltration performance. In addition, diffusion of small glucose molecules (0.66 nm) (Fig. 2f) into the large pores of selective pDA–TMC layers (Fig. S11) could well adjust the pore size distribution. The covalent bonding formed between glucose with the TMC and pDA endowed the membrane with significantly stability. Clearly, each of these components – pDA, UiO-66-NH$_2$ MOF, and glucose are synergistically essential

RESEARCH: Original Research

for creating a membrane with superior separation performances. The —NH$_2$ groups in UiO-66-NH$_2$ MOFs also enhanced the zeta potential of pDA–glucose selective layers by 84%, reaching −17 mV at pH = 7 (Fig. S12). Meanwhile, UiO-66 MOFs only increased the zeta potential of pDA–glucose membrane by 76%, from −105 mV to −25 mV at pH = 7. These results were in-line with the impact of chemical functionalization on the zeta potentials of UiO-66 MOFs [45]. Although the enhancing effect was much more pronounced at pH = 10, the membrane still showed a negative zeta potential surface from pH = 5 to pH = 10, which was the key to preferential rejection of negatively charged molecules by Donnan effects [46]. The incorporation of Zr-based MOFs also reduced the hydrophilicity of the pDA–glucose selective layer (Fig. S13). The water contact angle of pristine pDA–glucose selective layers was 18.1 ± 1° and was slightly enhanced to 25.3 ± 1.8 ° and 23.8 ± 1.5 ° in the presence of UiO-66-NH$_2$ and UiO-66 MOFs, respectively. Actually, all membranes were hydrophilicity and the contact angle were lower than the pristine porous substrate (38.5 ± 0.2°). Most importantly, the good hydrophilicity, endowed negative zeta potential and abundant intrinsic porosity of our utilized MOFs simultaneously contributed to the unprecedented separation performances of developed natural compound-based membranes.

The pDA played an equally important role for the performance of OSN membrane as it could quickly react with acyl-chloride groups at room temperature, improving distribution and enhance TMC loading on the membrane surface for subsequent interfacial polymerization [13]. To confirm the crucial role of pDA, we synthesized another TFN membrane without the pDA pre-coating via the same method. UiO-66-NH$_2$ MOFs agglomerated at sporadic localities within the glucose matrix (Fig. S14), while the separation performances of glucose/MOF nanocomposite membrane was non-ideal (Fig. 2g) with high permeance to ethanol (98.1 L m^{-2} h^{-2} bar^{-1}) and low rejection rate (42.5%) for Rose Bengal dyes. Although the pDA layer reduced ethanol permeance by 75%, the rejection rate was increased to nearly 100% and the ethanol permeance of 24.8 L m^{-2} h^{-2} bar^{-1} was comparable to state-of-the-art membranes [17,28]. This was due to the low abundance and non-uniform dispersion of TMC without pDA, which reduced glucose/UiO-66-NH$_2$ interface reaction. The longer pDA deposition duration led to the higher pDA content for making up the defects [13], which can underpin the significant increase in rejection rate and drastic loss in solvent permeance as the increased resistance to molecular transportation. Separation performances of different membranes with increasing the pDA coating time were shown in Fig. 2g. The permeance decreased dramatically as the pDA deposition time increased from 0 h to 12 h and the obvious color change can be observed (Fig. S14); while the rejection rate of solute increased. According to SEM and pore size distribution results (Fig. S15), prolonging the dopamine reaction time can lessen the defect formation of the synthesized membrane by increasing the UiO-66-NH$_2$ MOFs particles on the surface and decreasing the pore size. An ideal pDA coating duration (8 h) was required to optimize rejection rates by minimizing the formation of non-selective voids (Fig. 2g), whilst preventing macroscopic cracks during membrane fabrication and imbuing chemical stability to glucose in polar solvents.

Organic solvent nanofiltration experiments were performed at 5 bar and 25 °C. It was important to point out here that the fast solvent permeances of our pDA–glucose/MOF membranes was achieved with low pressures, voiding need to use the conventional energy-intensive high pressures for OSN operation [47]. Additionally, the use of low pressures can potentially further reduce the energy consumption of OSN. A range of polar solvents including methanol (MeOH), ethanol (EtOH), isopropanol (IPA), acetone, ethyl acetate (EA), Acetone, and dimethylformamide (DMF) was deployed to characterize molecular transport across pDA–glucose/MOF TFN membranes (Fig. 3a). The solvent permeances of pDA–glucose membranes studied here were significantly higher than our previously reported crosslinked pDA composite membrane. Polymer crosslinking usually reduces solvent transport because of denser structures [48]. UiO-66 and UiO-66-NH$_2$ MOFs enhanced solvent permeances without sacrificing selectivity towards dyes of different sizes, and charges. All solvent permeances including DMF were higher than 15 L m^{-2} h^{-1} bar^{-1} whilst rejecting more than 98% Rose Bengal. Amongst all membranes studied here, pDA–glucose/UiO-66-NH$_2$ membranes loaded with UiO-66-NH$_2$ MOFs possessed the best separation performances with both high permeance and good rejection rates. This could be attributed to the synergetic effects of glucose, UiO-66-NH$_2$ and pDA in the selective layer. The excellent compatibility between glucose and UiO-66-NH$_2$ inhibited the formation of non-selective pores within the selective layer. This effectively enhanced both solvent permeances and dye rejection rates. Hydrogen and amide bonding between functional groups of the UiO-66-NH$_2$ and glucose attributed to the fine dispersion of additional molecular transport pathways arising from the intrinsic porosity of well-dispersed UiO-66-NH$_2$. Meanwhile, as the UiO-66-NH$_2$ pores were smaller than the dyes, enhancing solvent/dye selectivity. New covalent bonds between each component during interfacial reactions endowed the resultant ultra-thin membrane with unparalleled chemical resistance to harsh organic solvents such as DMF. In addition, the unique adhesion properties of pDA was harnessed here to prevent the delamination of the glucose/MOF selective layer from the porous substrate and reduced macroscopic cracks during membrane fabrication.

The DMF permeance of pDA–glucose/UiO-66-NH$_2$ membranes reached 15.5 L m^{-2} h^{-1} bar^{-1}, significantly higher than that of thin polyamide [49] and TiO$_2$ membranes [50]. The separation performances of our membranes were characterized using polar protic (EtOH) and aprotic (DMF) systems that contained a series of dye molecules with different sizes (molecular weight ranging from 407 to 1017 Daltons) and charges (+1 to −2). Amongst all membranes studied here, pDA–glucose/UiO-66-NH$_2$ membranes demonstrated the highest DMF and EtOH permeances and highest dye rejection rates (Fig. 3b,c); surpassing state-of-the-art covalent organic framework membranes [51] and nanometer-thin membranes of polymers with enhanced microporosity [52]. The EtOH and acetone permeances of pDA–glucose/UiO-66-NH$_2$ membranes were further enhanced after DMF activation. EtOH permeance increased by 22%, from 24.8 L m^{-2} h^{-1} bar^{-1} to 30.2 L m^{-2} h^{-1} bar^{-1}, while acetone permeance was increased by 15% without compromising rejection rates (Fig. 3d). DMF activation removed small oligomeric/polymeric fragments trapped within the porous support;[53-56] gen-
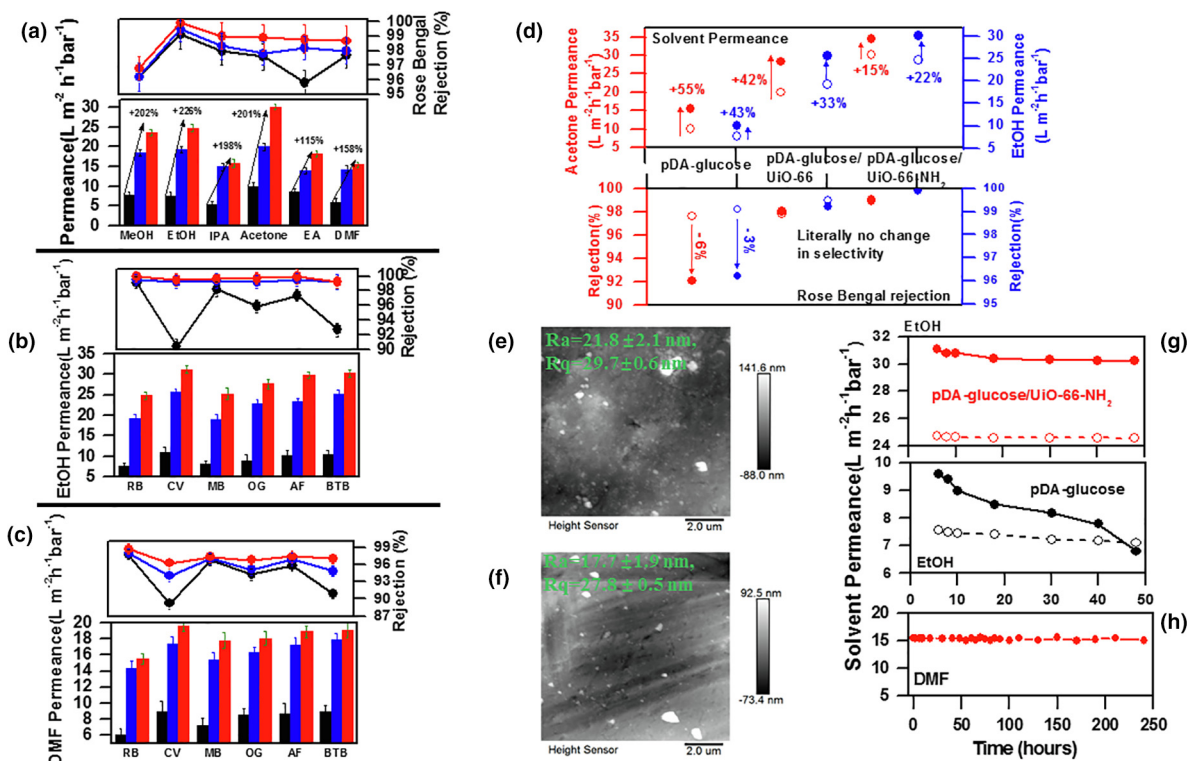
5

FIGURE 3

(a) Solvent permeance and RB rejection rates of pDA–glucose (black column/line), pDA–glucose/UiO-66(blue column/line) and pDA–glucose/UiO-66-NH₂ (red column/line) ultrathin nanocomposite membranes. The transport of solvent molecules (b) protic – EtOH and (c) aprotic – DMF across MOF-loaded TFN membranes. The rejection rates of various dyes in EtOH and DMF systems. (d) The EtOH and acetone permeances and RB rejection rates of the pDA–glucose, pDA–glucose/UiO-66, and pDA–glucose/UiO-66-NH₂ membranes before (blue hollow circle for EtOH, red hollow circle for acetone) and after (blue solid circle for ETOH, red solid circle for acetone) DMF activation. Change in surface roughness of pDA–glucose/UiO-66-NH₂ (e) before and (f) after DMF activation. (g) The time-dependent EtOH permeance of pDA–glucose and pDA–glucose/UiO-66-NH₂ membranes before (dotted line) and after (solid line) DMF activation. (h) The time-dependent DMF permeance of pDA–glucose/UiO-66-NH₂ (without activation) for DMF 240 h.

erating an open structure and structural rearrangement of the layer with optimized membrane structure, further enhancing solvent transport (Fig. 3e and f). The average roughness (Ra) and root mean square roughness (Rq) of pDA–glucose/UiO-66-NH₂ membranes reduced after DMF activation. During DMF immersion, the swollen selective layer can relax the undulated surface topological features, leading to structural rearrangement and reduced surface roughness [57]. Therefore, DMF activation manipulation of pDA–glucose/UiO-66-NH₂ membrane could further enhance the solvent permeances by maintaining dye rejection rates compared with the membranes without MOF nanoparticles. The excellent separation performances of pDA–glucose/MOF membranes studied here were maintained in continuous long-term operation for 50 h of EtOH before/after DMF activation and 240 h for DMF; highlighting performance longevity (Fig. 3g and h). This was different from traditional membranes comprising thin polyamide selective layers [54] that were prone to physical aging effects. This was probably due to the anti-aging capabilities of polydopamine [58]. Hydrogen bonding and chemical bond between UiO-66-NH₂ MOFs and the biopolymer chains might also immobilize glucose chains.

Interestingly, the incorporation of UiO-66-NH₂ MOFs into the pDA–glucose selective layer greatly increased NaCl rejection rate to 92.3%, whilst simultaneously enhancing water permeance by 114.8% (from 18.3 L m⁻² h⁻¹ bar⁻¹ to 39.3 L m⁻² h⁻¹ bar⁻¹)

(Fig. 4a). By contrast, a pDA–glucose membrane only demonstrated a NaCl rejection rate of 79.2% (at pH = 7). This observed increment in water permeance could be ascribed to the intrinsic porosity of MOFs that provided additional pathways for water transport. Meanwhile, enhanced rejection rates were attributed to the thicker separation layer and the relatively small pore radius (0.30 nm) which was smaller than the radii of hydrated ions (0.33–0.5 nm) (Fig. 4b) [59]. The selectivity of pDA–glucose/UiO-66-NH₂ membranes to 1000 ppm of inorganic salts was in the order of Na₂SO₄ (99.9%) > MgSO₄ (98.9%) > MgCl₂ (97.4%) > NaCl (92.3%). The rejection rate of inorganic salt was closely related to the chargeability of membranes and ion sizes. The charge on the membrane surface was characterized by zeta-potential tests, and the composite membrane with the larger zeta-potential had a greater electrostatic repulsion effect on the same charged ions by the Donnan exclusion [46]. The typical pDA–glucose/UiO-66-NH₂ nanofiltration membranes was negatively charged from pH = 5 to pH = 10 on the surface as described above. The high rejection rate of the divalent anion SO_4^{2-} of pDA–glucose/UiO-66-NH₂ nanocomposite membranes was ascribed to the electrostatic interaction between the negatively charged membranes and divalent anions, and also the larger radii of hydrated anions (0.43 nm). The synergistic effect of size sieving and Donnan exclusion underpinned high salt rejection rates [60] in these membranes. Crucially, the high salt rejection rates
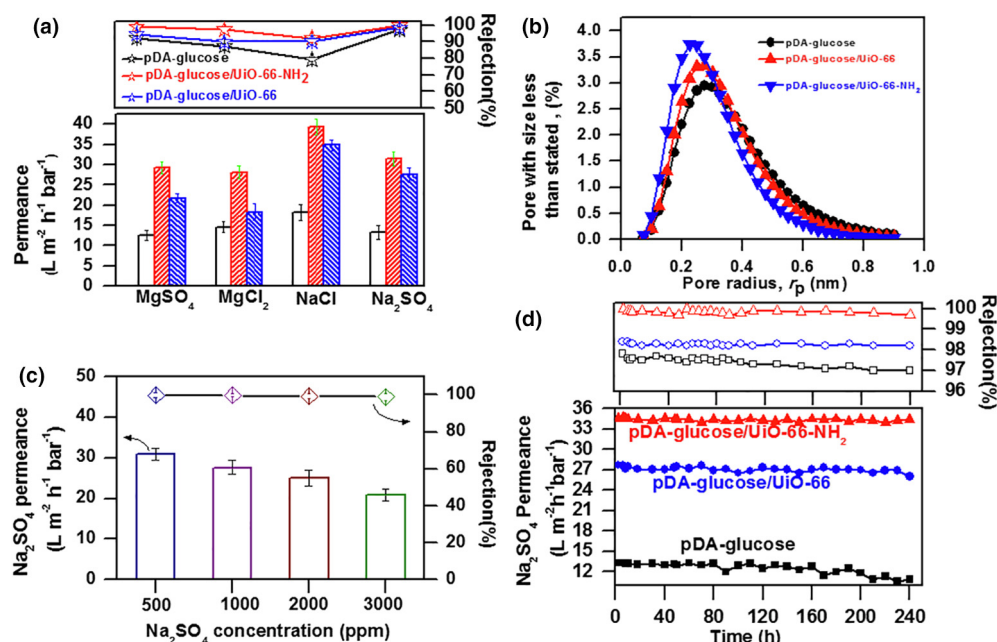
RESEARCH: Original Research

FIGURE 4

(a) Permeance and rejection rates of pDA–glucose, pDA–glucose/UiO-66, and pDA–glucose/UiO-66-NH$_2$ membranes for inorganic salts aqueous solution. (b) The pore size distribution of the pDA–glucose, pDA–glucose/UiO-66, and pDA–glucose/UiO-66-NH$_2$ membranes. (c) Effects of Na$_2$SO$_4$ concentrations on the performance of pDA–glucose/UiO-66-NH$_2$ membranes. (d) The time-dependent permeance and rejection rates of pDA–glucose, pDA–glucose/UiO-66 and pDA–glucose/UiO-66-NH$_2$ membranes in 1000 ppm Na$_2$SO$_4$ aqueous solution.

did not compromise water permeance. Compared to state-of-the-art MOF-based nanocomposite and other high performance nanofiltration membranes, the high salt rejection rates of our pDA–glucose/UiO-66-NH$_2$ membranes were significantly higher (Table S6) [26,61–66]. Even in the presence of 3000 ppm Na$_2$SO$_4$, the water permeances of pDA–glucose/UiO-66-NH$_2$ membranes reached 20.9 L m^{-2} h^{-1} bar^{-1} with 99% rejection (Fig. 4c). As desired, this membrane demonstrated extraordinary stable water filtration performance (Fig. 4d) benefiting from the exceptional stability of UiO-66-NH$_2$ MOF additives. No discernible degradation of membrane performance was observed during the tests around 240 h with saline solutions at the transmembrane pressure of 5 bar, further highlighting the multi-functionality of our membrane.

The separation performances of pDA–glucose/UiO-66-NH$_2$ membranes were also resistant to biofouling – a common cause underpinning performance loss due to the build-up of bio-matter on membrane surfaces (Fig. S16). Anti-fouling properties of membranes studied here were evaluated using three-cycle filtration tests and aqueous solutions containing 1 g/L of bovine serum albumin (BSA) or humic acid (HA) for 1200 min. The flux recovery ratios (FRR) of pDA–glucose/UiO-66-NH$_2$ membranes after three cycles were still 90.9% (BSA solution) and 94.9% (HA solution) with complete rejection rates and the lower total fouling ratios (DRt) (22.0% for BSA solution and 15.1% for HA solution) were observed. The excellent resistance towards these hydrophobic biomolecules was due to the hydrophilic nature of the negatively-charged pDA–glucose/UiO-66-NH$_2$ membrane [67,68]. Additionally, as both BSA and HA molecules are also negatively-charged, the Donnan exclusion mechanism also contributed towards anti-biofouling characteristics [69,70]. Besides

the good resistance towards biofouling and excellent long-term operation stability, our pDA–glucose/UiO-66-NH$_2$ membranes also demonstrated excellent thermal (Fig. S17) and mechanical (Fig. S18) stabilities. UiO-66-NH$_2$ MOFs can enhance the thermal stability of pDA–glucose matrices by 50 °C. This could be ascribed to strong hydrogen bonding and covalent bond between the glucose matrix and UiO-66-NH$_2$ MOFs, which was typical of these nanocomposites [41]. Compared to pDA–glucose membranes, hydrogen bonding and covalent bonding between glucose and UiO-66-NH$_2$ MOFs also underpinned the 45% increment in tensile strength, from 2.69 ± 0.1 MPa to 3.89 ± 0.1 MPa and a 170% increment in Young's modulus increased (from 38 ± 0.5 MPa to 108 ± 0.3 MPa). UiO-66-NH$_2$ MOFs enhanced the storage modulus of pDA–glucose matrices across a temperature range (Fig. S19), indicative of excellent mechanical stability [71] in our designed MOF-loaded nanocomposite membranes.

Conclusion

In summary, we have developed a new, extendable protocol utilizing materials from sustainable natural compounds to fabricate multi-functional, high-performance TFN membranes for fluid precise purification via different modes of nanofiltration. The interfacial polymerization reactions of natural compounds in the presence of compatible MOF additives on the surface of synthetic porous substrates formed ultrathin selective layers. These ultrathin composite membranes derived from natural compounds were highly permeable whilst demonstrating excellent chemical stability. We demonstrated the multi-functionality of this membrane through realistic experimental measurements of solvent permeance and molecular/salt rejection rate during organic solvent nanofiltration and low-pressure desalination.

7

Besides the excellent desalination performance, the solvent permeances of these sustainable ultrathin nanocomposite membranes greatly outperformed state-of-the-art membranes and two orders of magnitude higher than that of commercially OSN membrane. This was mainly ascribed to the synergistic effects of each component that overcome the traditional drawbacks of polymers from natural compounds – poor chemical stability, low solvent permeance and reduced selectivity. Importantly, our designed strategy can be extended to other polyphenols and natural compounds with compatible functionality to produce next-generation membranes with a plethora of combinations.

Conflict of interest

All authors have no conflict of interest.

CRediT authorship contribution statement

Yanqiu Zhang: Conceptualization, Writing - original draft, Writing - review & editing. **Xiquan Cheng:** Writing - review & editing. **Xu Jiang:** Writing - review & editing. **Jeffrey J. Urban:** Writing - review & editing. **Cher Hon Lau:** Writing - original draft, Writing - review & editing. **Shaoqin Liu:** . **Lu Shao:** Supervision, Conceptualization, Writing - original draft, Writing - review & editing.

Data availability

Experimental data from this study are available from Dr. Yanqiu Zhang and from Pro. Lu Shao (email: shaolu@hit.edu.cn) upon reasonable request.

Appendix A. Supplementary data

Supplementary data to this article can be found online at https://doi.org/10.1016/j.mattod.2020.02.002.

References

[1] X. You et al., Nat. Commun. 10 (2019) 4160.
[2] R. Zhang et al., Chem. Soc. Rev. 45 (2016) 5888–5924.
[3] D.S. Sholl, R.P. Lively, Nature 532 (2016) 435+.
[4] J. Hou et al., Adv. Mater. (2019) 1902009.
[5] X. He et al., Adv. Funct. Mater. 29 (2019) 1900134.
[6] S. Loeb, Science 147 (1965) 1241–1242.
[7] R.A. Gross, B. Kalra, Science 297 (2002) 803–807.
[8] P.R. Gruber, (2001) 166–184.
[9] K. Rohrbach et al., Chem. Commun. 50 (2014) 13296–13299.
[10] L. Huang et al., Adv. Mater. 28 (2016) 8669–8674.
[11] B. Liang et al., Adv. Mater. (2019) 1806090.
[12] Y. Zhang et al., J. Membr. Sci. 429 (2013) 235–242.
[13] H.-C. Yang et al., Adv. Funct. Mater. 28 (2018) 1705327.
[14] Z. Wang et al., Matter 1 (2019) 115–155.
[15] B.M. Ganesh et al., Desalination 313 (2013) 199–207.
[16] S. Kim et al., J. Mater. Chem. A 5 (2017) 1533–1540.
[17] S. Basu et al., J. Membr. Sci. 344 (2009) 190–198.
[18] C.H. Lau et al., Angew. Chem. Int. Ed. 53 (2014) 5322–5326.
[19] M.F. Haase et al., Nature Commun. 8 (2017) 1234.
[20] H.-C. Zhou et al., Chem. Rev. 112 (2012) 673–674.
[21] N.C. Su et al., Energy Environ. Sci. 9 (2016) 922–931.
[22] C.H. Lau et al., Angew. Chem. Int. Ed. 54 (2015) 2669–2673.
[23] J. Campbell et al., J. Mater. Chem. A 3 (2015) 9668–9674.
[24] J. Campbell et al., J. Mater. Chem. A 2 (2014) 9260–9271.
[25] J. Yao, H. Wang, Chem. Soc. Rev. 43 (2014) 4470–4493.
[26] X. Liu et al., J. Am. Chem. Soc. 137 (2015) 6999–7002.
[27] D. Ma et al., ACS Appl. Mater. Interfaces 11 (2019) 45290–45300.
[28] S. Sorribas et al., J. Am. Chem. Soc. 135 (2013) 15201–15208.
[29] Y. Li et al., Chem. Commun. 51 (2015) 918–920.
[30] X. Cheng et al., ACS Appl. Mater. Interfaces 9 (2017) 38877–38886.
[31] Y. Li et al., J. Mater. Chem. A 7 (2019) 19269–19279.
[32] C.X. Yan et al., J. Membr. Sci. 497 (2016) 77–89.
[33] H.M. Tham et al., ChemSusChem 11 (2018) 2612–2619.
[34] M.J. Katz et al., Chem. Commun. 49 (2013) 9449–9451.
[35] Z.F. Gao et al., J. Membr. Sci. 574 (2019) 124–135.
[36] M.R. DeStefano et al., Chem. Mater. 29 (2017) 1357–1361.
[37] H. Lee et al., Proc. Natl. Acad. Sci. U.S.A. 103 (2006) 12999–13003.
[38] J. Zhao et al., J. Mater. Chem. A 3 (2015) 19980–19988.
[39] J.H. Cavka et al., J. Am. Chem. Soc. 130 (2008) 13850–13851.
[40] Z. Wenjuan et al., Phys. Chem. Chem. Phys. 14 (2012) 2317–2325.
[41] M. Golpour, M. Pakizeh, Chem. Eng. J. 345 (2018) 221–232.
[42] B. Ghalei et al., Nature Energy 2 (2017) 17086.
[43] S.R. Venna et al., J. Mater. Chem. A 3 (2015) 5014–5022.
[44] Z. Wang et al., J. Mater. Chem. A 5 (2017) 10968–10977.
[45] Q. Chen et al., Appl. Surf. Sci. 327 (2015) 77–85.
[46] P. Marchetti et al., Chem. Rev. 114 (2014) 10735–10806.
[47] E.M. Rundquist et al., Green Chem. 14 (2012) 2197–2205.
[48] I.B. Valtcheva et al., J. Membr. Sci. 457 (2014) 62–72.
[49] M.F.J. Solomon et al., J. Membr. Sci. 434 (2013) 193–203.
[50] I. Soroko, A. Livingston, J. Membr. Sci. 343 (2009) 189–198.
[51] S. Kandambeth et al., Adv. Mater. 29 (2017) 1603945.
[52] M.F. Jimenez-Solomon et al., Nat. Mater. 15 (2016) 760–767.
[53] J.M. Hutchinson, Prog. Polym. Sci. 20 (1995) 703–760.
[54] I. Rose et al., Nat. Mater. 16 (2017) 932.
[55] S. Karan et al., Science 348 (2015) 1347–11351.
[56] M.F. Jimenez Solomon et al., J. Membr. Sci. 423–424 (2012) 371–382.
[57] J. Kurchan, Nature 433 (2005) 222.
[58] S.L. Phua et al., Acs Appl. Mater. Interfaces 5 (2013) 1302–1309.
[59] L. Yu et al., Angew. Chem. Int. Ed. 57 (2018) 172–178.
[60] T. Wang et al., J. Membr. Sci. 511 (2016) 65–75.
[61] G. Bargeman et al., Sep. Purif. Technol. 134 (2014) 46–57.
[62] Z. Tan et al., Science 360 (2018) 518–521.
[63] J. Zhu et al., ACS Appl. Mater. Interfaces 9 (2017) 1975–1986.
[64] H. Yi et al., Adv. Funct. Mater. 23 (2013) 3693–3700.
[65] Z. Yuzhang et al., Small 12 (2016) 5034–5041.
[66] Y.J. Tang et al., J. Membr. Sci. 498 (2016) 374–384.
[67] A.K. Shukla et al., Sci. Rep. 7 (2017) 41976.
[68] R.N. Zhang et al., J. Membr. Sci. 566 (2018) 258–267.
[69] H.G. Sun et al., J. Membr. Sci. 563 (2018) 22–30.
[70] D. Guo et al., J. Colloid Interf. Sci. 560 (2020) 273–283.
[71] K. Dey et al., Angew. Chem. Int. Ed. (2019) 201912381.